

Telecommand/Telemetry Ranging for Deep-Space Applications

Victor Vilnrotter
Jet Propulsion Laboratory
California Institute of Technology
4800 Oak Grove Dr.
Pasadena, CA 91109
818-354-2745
Victor.A.Vilnrotter@jpl.nasa.gov

Jon Hamkins
Jet Propulsion Laboratory
California Institute of Technology
4800 Oak Grove Dr.
Pasadena, CA 91109
818-354-4464
Jon.Hamkins@jpl.nasa.gov

Abstract— Conventional two-way pseudonoise (PN) ranging relies on measuring the time delay between a PN signal transmitted to the spacecraft, and a corresponding synchronized PN signal transmitted from the spacecraft and received on the ground. Recently, we introduced a two-way ranging method ([1], [2], [3]) which eliminates the need for the downlink PN ranging signal. In this telemetry ranging scheme, the requisite timing measurements are obtained from a data-bearing downlink telemetry signal. In the present paper, we extend the telemetry ranging concept by also eliminating the uplink PN signal, which is replaced by a data-bearing telecommand signal. We describe the architecture and concept of such a system, and describe the fundamental limitations of tracking the timing of such uplink telecommand signals when tracking loops or demod-remod correlation techniques are employed. An end-to-end performance analysis shows that in typical scenarios, ranging performance comparable to conventional PN ranging is possible.

TABLE OF CONTENTS

1. INTRODUCTION.....	1
2. TELECOMMAND RANGING.....	2
3. SIGNAL MODEL	2
4. ML DELAY ESTIMATION	3
5. CRAMER-RAO BOUNDS.....	4
6. CODEWORD AIDED DELAY ESTIMATION.....	4
7. NUMERICAL RESULTS.....	5
8. WINDOWING TO IMPROVE PERFORMANCE.....	7
9. END-TO-END RANGING ACCURACY.....	8
10. SUMMARY AND CONCLUSIONS	9
ACKNOWLEDGEMENTS	10
REFERENCES.....	10

1. INTRODUCTION

NASA's deep-space missions primarily rely on sequential ranging [4] to determine the distance, or range, between reference points on the ground and spacecraft antennas. In the typical design, a non-regenerative approach is used, in which a sequence of sinusoids, or tones, is transmitted from the ground to the spacecraft. The spacecraft uses the demodulated signal, with its noise, to modulate the downlink

carrier. Conceptually, the signal makes a round trip from the ground to the spacecraft and back to the ground, and at sufficient SNR the two-way delay may be readily determined. Because the noise on the uplink is present in the downlink transmission, such a scheme has a performance proportional to $1/R^4$, where R is the range to the spacecraft.

A number of years ago, a regenerative pseudonoise (PN) ranging approach was suggested [5]. In this scheme, a PN-like signal is transmitted from the ground to the spacecraft, which acquires its timing with sufficient accuracy so as to regenerate an onboard copy of the PN sequence, synchronous with the received PN signal. The local copy is used to modulate a downlink carrier. Since no noise is present on the spacecraft-regenerated PN signal, the performance of the regenerative approach is proportional to $1/R^2$. New Horizons was the first spacecraft to demonstrate PN ranging using the Deep Space Network [6].

More recently, an extension of PN ranging was developed in which the downlink PN transmission is replaced with a data-bearing telemetry signal [1]. In this telemetry ranging scheme, the PN signal is transmitted from the ground to the spacecraft, which acquires its timing, the same as in conventional PN ranging. The spacecraft then records the location within the PN sequence, or PN phase, that it sees in this uplink PN signal at the precise moment it transmits the first symbol of a data frame in its downlink telemetry. By tracking the Earth time-of-arrival of the data frame, and with suitable processing [2], the same two-way measurement of delay can be made. Telemetry ranging helps increase telemetry data volume because no spacecraft power is used to transmit a dedicated ranging signal, and no ranging signal is present to interfere with the telemetry signal.

In the present paper, we extend the telemetry ranging concept by eliminating the uplink PN transmission as well. In this telecommand/telemetry ranging concept, the uplink transmission is a data-bearing telecommand signal. With this new concept, neither the uplink nor the downlink uses a PN transmission.

2. TELECOMMAND RANGING

Uplink

Currently, when a deep-space NASA mission needs to telecommand the spacecraft, the ground transmits a sequence of Communications Link Transmission Units (CLTUs), in accordance with the CCSDS telecommand (TC) protocol [7]. Each CLTU comprises a start sequence, a number of codewords, and-possibly a tail sequence. Any gaps between CLTUs are filled with an idle sequence. In telecommand/telemetry ranging, this transmission protocol is unchanged. The only new thing is that the ground records the time the CLTUs are transmitted, along with the Frame Sequence Number present in the primary header of the first TC Transfer Frame of the CLTU. The structure of the CLTU and the Frame Sequence Number within it are illustrated in Fig. 1.

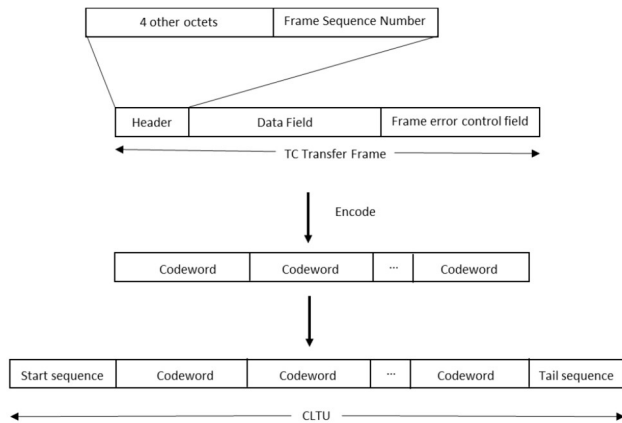


Figure 1. The Frame Sequence Number is located in the header of the TC Transfer Frame, which is encoded into one or more codewords within a CLTU.

Downlink

On the spacecraft, the telecommand is demodulated and decoded in the usual way. What is important for telecommand/telemetry ranging is to make an association between which symbol of the uplink is arriving at the moment the downlink is transmitting the first symbol of a telemetry frame. In our proposed scheme, the spacecraft keeps a continuous count of the integer and fractional number of symbols which have arrived since the beginning of the last received CLTU, along with the Frame Sequence number present in the primary header of the first TC Transfer Frame of this CLTU. (Our proposed ranging scheme is compatible with potential gaps between CLTU transmissions, during which an idle sequence is transmitted [7].) At the moment that a downlink telemetry frame is transmitted, this uplink

symbol-count is latched and stored, along with the Frame Sequence Number of the uplink TC frame and Frame Counter of the TM frame. These pairs are sent to the ground as telemetry, in a subsequent telemetry frame.

Range Computation

On the ground, the Earth time-of-arrival of the telemetry frames are recorded, as in telemetry ranging. The delay between the uplink CLTU transmission and receive time of the telemetry frame is computed. The auxiliary information recorded on the spacecraft assures that each telemetry frame will be associated with the appropriate CLTU to ensure the accuracy of the delay computation.

Spacecraft Measurement Accuracy

Often, the data rate and symbol SNR of the uplink command is low. This can correspond to limited capability of timing resolution on the spacecraft. Therefore it is incumbent on us to show that methods exist to recover the timing with sufficient accuracy in practical scenarios.

Several approaches can be applied to aid the arrival-time estimation process via the demod-remod process, by making use of the information contained in the decoded codewords (assuming error-free decoding, as would be the case under normal operating conditions). In this paper, we examine sample-by-sample correlation of the received CLTU with the perfect stored copy, obtained via the demod-remod operation, similar to correlation estimation of delay with pseudonoise (PN) sequences when the received PN sequence is known.

3. SIGNAL MODEL

The phase-modulated signal received at the spacecraft can be expressed as $s(t) = \text{Re} \left(A \exp \{ j[\omega_0 t + \phi s(t - \tau) + \theta] \} \right)$, where A is the received signal amplitude, τ is the uplink delay, ω_0 is the carrier frequency, ϕ is the modulation index, θ is an unknown carrier phase, and $s(t - \tau) = \sum_i d_i p(t - \tau)$ is the data-modulated uplink command sequence where $d_i = \pm 1$ is a random binary sequence and $p(t)$ is a pulse-shape usually selected for favorable spectral characteristics of the transmitted signal. Following complex downconversion at the spacecraft, the carrier frequency is eliminated and the carrier phase driven towards zero via a carrier tracking loop, either locking onto a residual carrier or by means of a Costas loop, yielding the complex phase-modulated waveform

$$\begin{aligned} A \exp \{ j[\phi s(t - \tau)] \} &= A \{ \cos[\phi s(t - \tau)] + j \sin[\phi s(t - \tau)] \} \\ &= A [s_R(t - \tau) + j s_I(t - \tau)] \end{aligned}$$

This effectively assumes that the receiver has accurate estimates of the carrier phase such that $\hat{\theta} \cong \theta$, and that the received signal has been counter-rotated prior to detection, yielding $\exp[j(\theta - \hat{\theta})] \cong 1$. For the special case of unit-amplitude square pulses and a modulation index of $\phi = \pi / 2$

, the real part S_R (cosine term) is zero for either sign of the data, and the imaginary part S_I (sine term) reduces to $s(t - \tau)$, hence for this special case the signal can be fully recovered from the imaginary part of the phase-modulated signal: $s_{R,\phi=\pi/2} = \sin[\phi s(t - \tau)] \stackrel{\phi=\pi/2}{=} s(t - \tau)$. However this

is not true in general, since filtered phase-modulated signals project components onto both the real and imaginary components, and hence require a complex baseband model for complete characterization.

In the following examples, the BPSK waveform is modulated onto the Q component, taking on phase values of 0 and 180 degrees. Three types of BPSK waveforms are in common use: 1) unfiltered “ideal” BPSK; 2) I-Q modulated filtered BPSK; and 3) phase-modulated filtered BPSK symbols. For the unfiltered case, both modulator types yield waveforms identical to the unfiltered case. The key distinction between IQ and phase modulated waveforms is that with IQ modulation there is no cross-coupling between the I and Q components, hence the BPSK waveform occurs in only one of the IQ components (typically the Q component); however, the filtered IQ waveform is typically not a constant envelope waveform. Filtered phase modulated waveforms are constant envelope, however there is significant cross-coupling between the I and Q components, mathematically required to maintain constant phasor magnitude, or equivalently to keep the envelope of the transmitted fields constant.

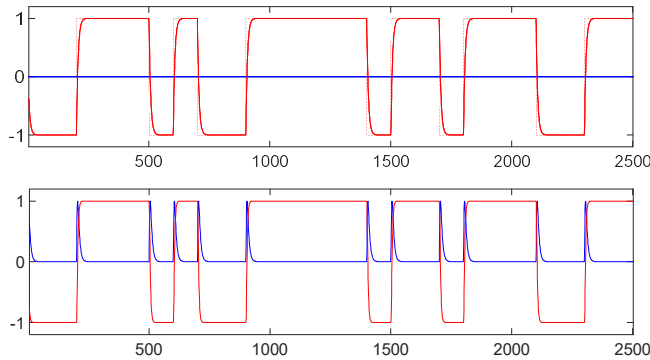


Figure 1. a) I-Q modulated unfiltered Q component (dashed red), I component (blue) and filtered Q (solid red) BPSK; b) phase-modulated filtered BPSK showing coupling between I (blue) and Q (red) components.

Higher dimensional QPSK and OQPSK signals behave similarly, but yield more complex waveforms since both I and Q components are modulated simultaneously. For the filtered and unfiltered IQ modulated waveforms I component (blue) is not zero, as with BPSK, but contains an independent data-stream. However, the filtered phase-modulated waveforms show complicated cross-coupling between the two components, as required mathematically to keep the magnitude of the phasor constant as it rotates to the next point in the signal constellation.

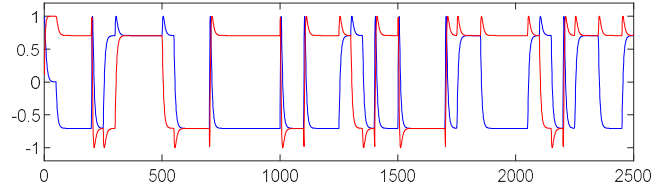


Figure 2. Filtered phase-modulated OQPSK, showing complex interaction between the I component (blue) and the Q component (red), as the phasor rotates within the constellation.

An example of filtered phase-modulated OQPSK signal is shown in Fig. 2, where the signal-constellation is located at $\pm 45, \pm 135$ degrees, and the spikes are generated as the phasor transitions between these angles, but necessarily rotating through 0, 90, and 180 degrees when filtered, hence generating large spikes.

4. ML DELAY ESTIMATION

The structure of the maximum likelihood estimator can be derived by maximizing the derivative of the likelihood function with respect to the parameter of interest. Following downconversion to complex baseband, the received signal can be modeled as an N -dimensional vector of complex baseband samples taken at integer multiples of the sampling interval Δt : $\tilde{r}(i\Delta t) = \tilde{s}(i\Delta t) + \tilde{n}(i\Delta t)$. Here, $\tilde{n}(i\Delta t)$ are assumed complex Gaussian noise samples with variance equal to the sum of the real and imaginary noise components: $\sigma_n^2 = \sigma_{n,R}^2 + \sigma_{n,I}^2$. Although important in deriving the signal model and noise statistics, the sampling interval Δt will be assumed known in the subsequent analysis and hence can be suppressed, yielding the simpler representation $\tilde{r}_i = \tilde{s}_i(\tau) + \tilde{n}_i$ (the delay τ has been incorporated into the signal samples to emphasize that this is the parameter to be estimated). The vector of N complex received samples can be represented in terms of signal and noise components as $\tilde{\mathbf{r}} = (\tilde{r}_0, \tilde{r}_1, \dots, \tilde{r}_{N-1})$, $\tilde{\mathbf{s}}(\tau) = [\tilde{s}_0(\tau), \tilde{s}_1(\tau), \dots, \tilde{s}_{N-1}(\tau)]$, and $\tilde{\mathbf{n}} = (\tilde{n}_0, \tilde{n}_1, \dots, \tilde{n}_{N-1})$. The real and imaginary noise samples are assumed to be independent with identical component variance, $\sigma_{n,R}^2 = \sigma_{n,I}^2$, and total variance σ_n^2 . The joint probability density of the complex noise vector is the product of the individual noise densities, assumed to be circular Gaussian densities:

$$\mathcal{P}(\tilde{\mathbf{n}}) = (\pi \sigma_n^2)^{-N} \prod_{i=0}^{N-1} \exp(-|\tilde{n}_i|^2 / \sigma_n^2) \quad (2)$$

Given the signal delay τ , the joint probability density of the received vector, conditioned on the signal parameter vector, can be expressed as:

$$\mathcal{P}(\tilde{\mathbf{r}} | \tau) = (\pi \sigma_n^2)^{-N} \prod_{i=0}^{N-1} \exp(-|\tilde{r}_i - \tilde{s}_i|^2 / \sigma_n^2) \quad (3)$$

The maximum likelihood (ML) estimate of the delay is that value that maximizes the conditional joint density in equation (2), or equivalently its natural logarithm, known as the log-likelihood function $\Lambda(\tilde{\mathbf{r}} | \tau) \equiv \ln[\mathcal{P}(\tilde{\mathbf{r}} | \tau)]$:

$$\Lambda(\tilde{\mathbf{r}}|\tau) = -N \ln(\pi \sigma_n^2) - \frac{1}{\sigma_n^2} \sum_{i=0}^{N-1} |\tilde{r}_i - \tilde{s}_i^*(\tau)|^2 \quad (4)$$

where * denotes conjugation. The received complex signal-plus-noise samples are denoted by \tilde{r}_i , while $\tilde{s}_i(\tau)$ represents the reconstructed codeword obtained via the demod-remod process. Expanding the square term in the sum yields

$$\begin{aligned} \Lambda(\tilde{\mathbf{r}}|\tau) &\equiv \ln[\mathcal{P}(\tilde{\mathbf{r}}|\tau)] = -N \ln(\pi \sigma_n^2) - \frac{1}{\sigma_n^2} \sum_{i=0}^{N-1} |\tilde{r}_i - \tilde{s}_i^*(\tau)|^2 \\ &= -N \ln(\pi \sigma_n^2) - \frac{1}{\sigma_n^2} \sum_{i=0}^{N-1} \{|\tilde{r}_i|^2 + |\tilde{s}_i^*(\tau)|^2 - 2 \operatorname{Re}[\tilde{r}_i \tilde{s}_i^*(\tau)]\} \end{aligned} \quad (5)$$

The maximum likelihood estimate of the delay τ is that value, $\hat{\tau}$, that maximizes the log-likelihood function $\Lambda(\tilde{\mathbf{r}}|\tau)$. For a given received vector $\tilde{\mathbf{r}}$ and reconstructed signal vector $\tilde{\mathbf{s}}(\tau)$, the terms $\sum_{i=0}^{N-1} |\tilde{r}_i|^2 = \mathcal{E}_r$ and $\sum_{i=0}^{N-1} |\tilde{s}_i(\tau)|^2 = \mathcal{E}_s$, respectively, are constants independent of τ hence do not impact the maximization and hence can be ignored. Likewise, the coefficients $-\sigma_n^{-2}$ and $2\sigma_n^{-2}$, and the term $-N \ln(\pi \sigma_n^2)$ can also be ignored in the maximization, yielding the following algorithm for estimating delay:

$$\hat{\tau} = \max_{\tau} \Lambda(\tilde{\mathbf{r}}|\tau) = \max_{\tau} \sum_{i=0}^{N-1} \operatorname{Re}[\tilde{r}_i \tilde{s}_i^*(\tau)] \quad (6)$$

The ML delay estimator specified in equation (6) computes the cross-correlation between the received noisy samples and the recovered signal vector. The modulation format has not been restricted in this derivation, hence equation (6) is equally valid for any modulation including ideal binary NRZ pulses, BPSK and QPSK and their filtered versions, or more complex continuous-phase modulations such as GMSK.

5. CRAMER-RAO BOUNDS

The Cramer-Rao lower bound (CRB) on the variance of delay estimation error is derived, assuming a known real signal corrupted by complex circular Gaussian noise. The estimation is based on N independent samples of the received signal-plus-noise and recovered signal vectors, as defined in Section III.

The CRB is again based on the log-likelihood function $\Lambda(\tilde{\mathbf{r}}|\tau)$, repeated here for convenience:

$$\Lambda(\tilde{\mathbf{r}}|\tau) = -N \ln(\pi \sigma_n^2) - \frac{1}{\sigma_n^2} \sum_{i=0}^{N-1} |\tilde{r}_i - \tilde{s}_i(\tau)|^2 \quad (7)$$

The CRB can be expressed in two different but equivalent forms. For delay estimation, these two forms are:

$$\operatorname{var}(\tau - \hat{\tau}) \geq \left(E \left\{ \left| \frac{\partial \Lambda(\mathbf{r}|\tau)}{\partial \tau} \right|^2 \right\} \right)^{-1} \quad (8a)$$

$$\operatorname{var}(\tau - \hat{\tau}) \geq \left(E \left\{ \left| \frac{\partial^2 \Lambda(\mathbf{r}|\tau)}{\partial \tau^2} \right| \right\} \right)^{-1} \quad (8b)$$

For the problem of estimating the delay of a known signal observed in the presence of additive noise, it is more convenient to square the first derivative of the log-likelihood

function, hence equation (8a) will be used in the following derivation. Taking the derivative of the log-likelihood function with respect to the delay τ , yields

$$\begin{aligned} \frac{\partial}{\partial \tau} \Lambda(\mathbf{r}|\tau) &= -\frac{1}{\sigma_n^2} \sum_{i=0}^{N-1} \frac{\partial}{\partial \tau} |\tilde{r}_i - \tilde{s}_i(\tau)|^2 \\ &= \frac{2}{\sigma_n^2} \sum_{i=0}^{N-1} [\tilde{r}_i - \tilde{s}_i(\tau)] \frac{\partial \tilde{s}_i(\tau)}{\partial \tau} = \frac{2}{\sigma_n^2} \sum_{i=0}^{N-1} \tilde{n}_i \frac{\partial \tilde{s}_i(\tau)}{\partial \tau} \end{aligned} \quad (9)$$

where the last equality follows from the fact that $\tilde{r}_i - \tilde{s}_i(\tau) = \tilde{n}_i$. Substituting and collecting terms, we obtain the following equation for the expected value of the square of the first derivative of the log-likelihood function:

$$\begin{aligned} E \left\{ \left| \frac{\partial}{\partial \tau} \Lambda(\mathbf{r}|\tau) \right|^2 \right\} &= \frac{4}{\sigma_n^4} E \left\{ \left| \sum_{i=0}^{N-1} \tilde{n}_i \frac{\partial \tilde{s}_i(\tau)}{\partial \tau} \right|^2 \right\} \\ &= \frac{4}{\sigma_n^4} \left\{ \sigma_n^2 \sum_{i=0}^{N-1} \left| \frac{\partial \tilde{s}_i(\tau)}{\partial \tau} \right|^2 + \sum_{i=0}^{N-1} \sum_{\substack{j=0 \\ j \neq i}}^{N-1} E(\tilde{n}_i \tilde{n}_j^*) \frac{\partial \tilde{s}_i(\tau)}{\partial \tau} \frac{\partial \tilde{s}_j^*(\tau)}{\partial \tau} \right\} \\ &= \frac{4}{\sigma_n^2} \sum_{i=0}^{N-1} \left| \frac{\partial \tilde{s}_i(\tau)}{\partial \tau} \right|^2 \end{aligned} \quad (10)$$

since $E(\tilde{n}_i \tilde{n}_j^*) = 0$ due to the statistical independence of the noise samples. Substituting into equation (8a) leads to the CRB for the error variance of any unbiased delay estimator:

$$\operatorname{var}(\tau - \tau') \geq \left(E \left\{ \left| \frac{\partial}{\partial \tau} \Lambda(\mathbf{r}|\tau) \right|^2 \right\} \right)^{-1} = \frac{\sigma_n^2}{4} \left(\sum_{i=0}^{N-1} \left| \frac{\partial \tilde{s}_i(\tau)}{\partial \tau} \right|^2 \right)^{-1} \quad (11)$$

Therefore, the lower bound on the error variance depends on the sample noise variance, and the inverse of the sum of squares of the derivative of the signal samples with respect to the delay. Since the signal is assumed to be known, this quantity can be calculated for any sequence of signal samples and substituted into equation (11) to obtain the CRB for delay estimation. Note that since the CRB derivation employed the complex baseband model, it remains equally valid for arbitrary phase-modulated or in-phase quadrature modulated (IQ) waveforms. In the next section, we develop and evaluate the performance of the delay estimator with filtered and unfiltered BPSK and QPSK signals.

6. CODEWORD AIDED DELAY ESTIMATION

Modern deep-space transponders such as the Small Deep-Space Transponder (SDST) and the USD, have the capability to demodulate, decode, re-encode and re-modulate data received on the uplink channel (also termed “demod-remod” for short), thus obtaining a noiseless, error-free copy of the received codeword in near-real-time. This new capability enables improved estimation of codeword arrival-time, which is the key parameter needed for two-way ranging applications, as described in previous articles on telemetry-based ranging [1,2,3,4]. However, since carrying out the steps of the demod-remod process takes time, likely on the order of micro-seconds but depending on the processing power on the spacecraft, the received noisy codeword samples must be stored for the duration of the codeword plus the processing

time, before the noise-free samples that are the result of the demod-remod process, become available. After the demod-remod process is complete, the noise-free samples can be clocked out together with the stored noisy samples, and with proper timing used to aid the arrival-time estimation of the received codeword.

It is assumed in the following development that the output of the demod-remod process is a noiseless error-free replica of the transmitted codeword (or sequence of codeword) samples, resampled and remodulated to accurately represent the signal samples embedded in the received signal. With ideal decoding of the received information-bearing codewords, as typical in operational uplink commands to spacecraft, the demod-remod process enables the treatment of the inherently random codewords as known waveforms. This added information further enables the designs of delay estimation algorithms that approach and even attain the lower bound on the variance of delay estimation error, as specified by the Cramer-Rao lower bound for the case of known waveforms, as derived in Section V.

As shown in Section IV, the structure of the maximum likelihood estimator with a known waveform consists of a correlator that computes the overlap integral of the received complex codeword samples with a sampled version of the demod-remod output for sample-delays within the uncertainty region, which can be considered a known waveform after error-free decoding. Although the block diagram for the remodulation section in Fig. 1 of the GMSK PN-Ranging Green Book shows a complex output, it can be argued that successful decoding of the received codeword requires accurate estimation of carrier phase and symbol delay. This implies that complex sampling may not be necessary, and hence only real samples of the phase-corrected and delay-compensated waveforms are required.

Although carrier phase and symbol delay must be estimated accurately for the decoder, phase errors of a tenth of a radian and symbol delay errors of a tenth of a symbol duration are generally adequate for accurate decoding. However, a delay error of a tenth of a symbol at the current uplink symbol-rate of 2 kbps corresponds to an rms delay error of 50 micro-sec, which translates to an rms range error of 150 km, clearly not acceptable for this application. Even at an uplink symbol-rate of 1 MSPS, an average delay error of a tenth of a symbol corresponds to 30 meters, which is not acceptable for this application. On the other hand, at an uplink symbol-rate of 100 MSPS, the rms error will only be 0.3 m which is consistent with the accuracy sought in this application. It appears that for symbol-rates greater than 100 MSPS the delay tracking algorithms typically employed in the DSN meet the requirements on range uncertainty required in the context of spacecraft navigation. It appears that for high symbol-rates conventional delay tracking or symbol synchronization algorithms such as the DTTL may suffice, unless future requirements demand even greater accuracy. However, for medium to low symbol-rates additional improvements to the on-board performance of the symbol

synchronization algorithms may be required to reach the desired sub-meter accuracy.

7. NUMERICAL RESULTS

The ML delay estimator based on the correlator structure derived in Section IV was simulated in MATLAB, applied to BPSK and OQPSK formats with filtered and unfiltered modulations either IQ modulated or phase-modulate onto the carrier, and compared to the CRB derived in Section V. The simulation generates random binary data-streams, sampled at a high enough to avoid aliasing, and to provide enough samples per symbol to simulate an analog signal near the pulse transitions, which is the critical region for delay estimation as shown by the form of the CRB. Real and imaginary Gaussian noise samples were added with variance chosen to establish a given sample signal-to-noise ratio, or *SNR*, defined as the ratio of sample energy to noise sample variance: $SNR = 2A^2 / \sigma_n^2$. Setting the signal amplitude to 1, the *SNR* takes on the simpler form $SNR = 1 / \sigma_{n,R}^2 = 1 / \sigma_{n,I}^2$, which is the SNR expression used in the simulation.

The sample SNR was increased from a minimum of -50 dB to +50 dB in 5 dB steps, to show estimator performance in three distinct regions: below threshold, in the intermediate range just above threshold, and in the high-SNR region where estimator performance should closely approach the CRB for an efficient unbiased estimator. Both BPSK and OQPSK modulations were simulated, with and without pre-modulation filtering, and delay estimator performance compared to the corresponding CRB to evaluate performance in all three regions of interest.

The structure of the ML algorithm derived in equation (6) was implemented in MATLAB. Delay was estimated by cross-correlating the received signal with the reference signal, taking the real part and finding the index of correlation delay (in samples) corresponding to the peak of the correlation function. In order to establish a time-base, the same process was followed using the auto-correlation function of the reconstructed reference signal. The delay estimate was computed as the difference between the reference signal auto-correlation peak, and the peak of the cross-correlation between the received and reference signals. An example of the auto-correlation (blue) and cross-correlation (red) functions is shown in Fig. 3 at sample-SNR of 15 dB, for IQ modulated filtered OQPSK signals at an applied delay of 53 samples with respect to the reconstructed reference signal, to show the separation of the peaks. Note that for such a high sample-SNR, and 10^4 samples per data-vector, the fluctuations in the correlation functions (off-peak) are due to the random data modulation, not additive noise, hence both functions are very nearly identical.

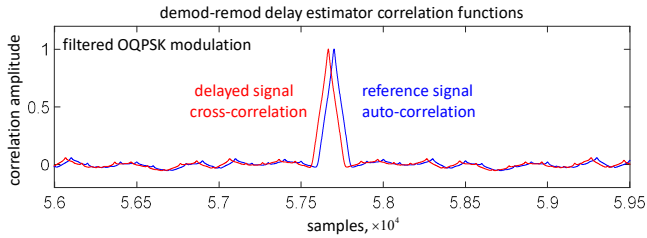


Figure 3. Filtered OQPSK auto-correlation function (blue) and cross-correlation function (red) at a sample-SNR of 15 dB; delay of 53 samples.

High SNR region

It was found that in the high-SNR region the rms delay errors became much smaller than the sampling interval, even when 100 samples per symbol were used.

Hence the resulting delay estimates tend to be very close to the input sample delay resulting in zero delay error even with a large number of simulations per delay estimate. Therefore, a quadratic interpolation algorithm was developed to refine the standard deviation of the delay estimates, using the location and value of the correlation peak and its two nearest neighbors, to refine the delay estimates to a small fraction of a sample.

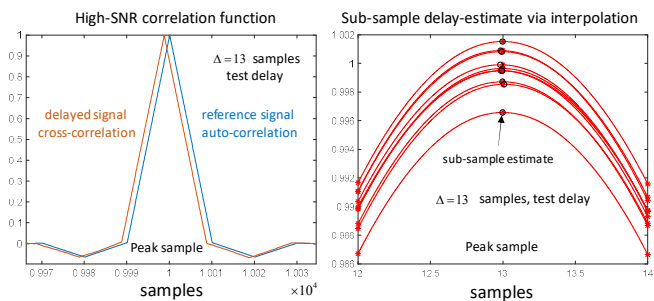


Figure 4. Correlation functions and fine delay estimates in the high-SNR regime.

Figure 4 shows the correlation function near the peaks, and the interpolation algorithm for a delay of 13 samples in the high-SNR region (above 0 dB sample-SNR). For this example, unfiltered BPSK modulation was used in order to simplify the plots.

Figure 4a) is a zoomed version of the correlation peaks for a delay of 13 samples, showing the two peaks separated by the correct number of integer samples. However, in order to obtain a non-zero error variance with a reasonable number of simulations (up to 10,000 simulations per point were tried, but the underestimates due to insufficient errors remained), the quadratic interpolation algorithm had to be invoked. It can be seen in Fig. 4b) that in a sequence of ten simulation points in this figure, the interpolated peaks (black circles) between the peak sample and its two nearest neighbors (red asterisks) that the interpolated values are very close to, but not exactly equal to the raw sample peaks. Hence the true delay variance can now be estimated with a reasonable number of simulations per point.

The performance of the delay estimator, measured in rms delay error, is shown in Fig. 7 for unfiltered BPSK and OQPSK signals. It can be seen that in the high-SNR region above 0 dB, the simulation points (black or blue asterisks) correspond very well to their respective CRBs (black or blue dashed lines), indicating efficient estimator performance that achieves the CRB.

Medium SNR region

The noticeable increase in rms delay error over the CRB in the intermediate region between -30 dB and zero dB sample-SNR in Fig. 7) can be understood by referring to Fig. 5. The zoomed correlation peaks in Fig. 5a) show a significant

degradation of the cross-correlation peak due to noise, as compared to the ideal auto-correlation peak of the reference signal. The true location of the cross-correlation peak is no longer obvious, and hence could be in error by a few samples. This leads to increased errors in the interpolated estimates, including occasional sample-level errors, as shown in Fig. 5b). The impact on delay estimation performance can be seen in Fig. 7, where the rms delay error in the intermediate region becomes noticeably larger than the CRB, showing an increase of approximately 3 dB (measured in terms of required sample-SNR).

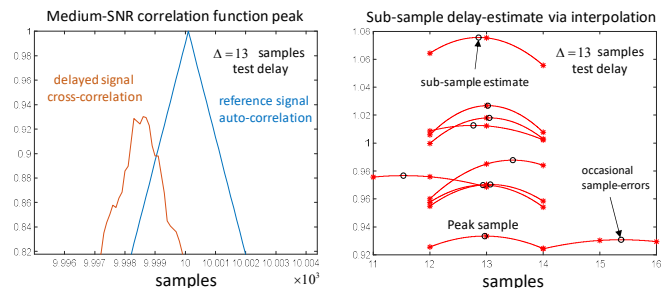


Figure 5. Correlation functions and fine delay estimates in the mid-SNR region.

Low SNR region

When the sample-SNR dips below -25 dB, a threshold effect occurs causing a great increase in delay estimation error. This effect is due to large outlier noise spikes that exceed the cross-correlation peak, which can occur anywhere in the delay uncertainty range, as can be seen in Fig. 6a where the largest cross-correlation peak is about 800 samples from the true delay. A few of these large outlier spikes will greatly increase the variance estimate, leading to the non-linear estimator behavior in the low-SNR region (below -25 dB) in Figs. 4. This non-linear behavior can be mitigated to some extent by limiting the delay search region to small values near the true delay, however this requires more accurate specification of the uncertainty range.

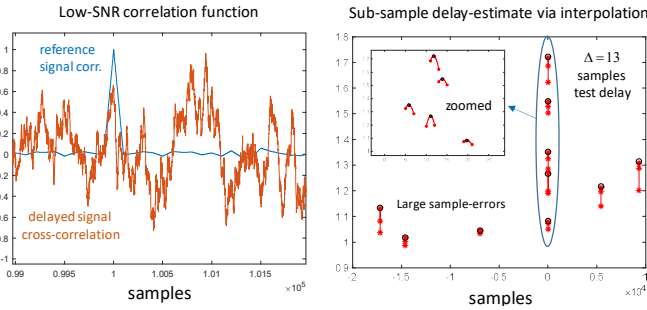


Figure 6. Correlation functions and fine delay estimates in the low-SNR region.

The performance curves in Fig. 7 were generated with 1000 simulations per point, in order to reduce the error-bar on the delay estimates to acceptable levels. Unfiltered BPSK and OQPSK signals were generated, and the error bars compared to the corresponding CRB obtained from equation (11), over all three SNR regions.

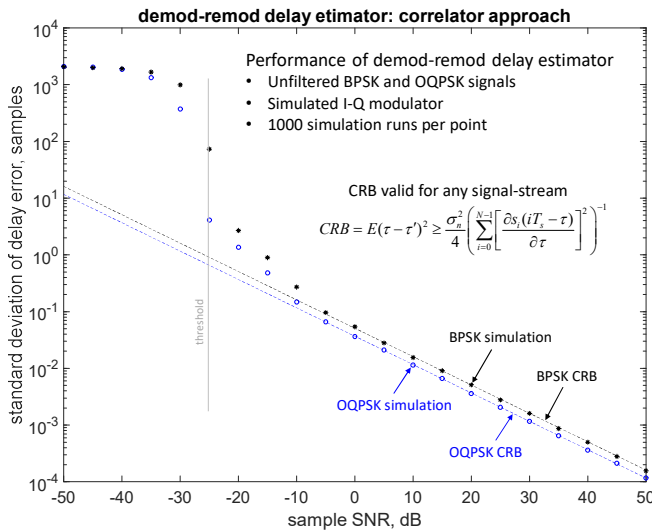


Figure 7. Comparison of ML delay estimator performance for unfiltered BPSK and OQPSK signals, with IQ modulation.

The performance of the delay estimator for BPSK and OQPSK shows 3dB improvement with OQPSK (blue) over BPSK (black), due to the fact that the complex noise variance is the same in both cases, but OQPSK has twice as many transitions as BPSK, hence the sum of the squared magnitude of the derivative is twice as great for OQPSK (or QPSK) as it is for BPSK, hence the CRB improves by 3 dB according to equation (11). It can be seen in Fig. 7 that the simulation points in the high-SNR region (0 dB to 50 dB sample-SNR) correspond well to the theoretical limit of the CRB, indicating efficient estimator performance in this region.

8. WINDOWING TO IMPROVE PERFORMANCE

The form of the CRB in equation (11) provides important insights into the structure of the delay estimator. Note that for any noise sample variance σ_n^2 , estimator performance depends entirely on the energy of the signal derivative, assumed to be known. For any known signal waveform, this

quantity can be calculated to determine the CRB, which remains constant for the same signal waveform, as in the case of PN ranging where the same PN sequence is transmitted repeatedly during the ranging measurements. In this application, the signal waveform consists of a CCSDS data-packet, called a CLTU, which has both a constant header and a random data-sequence: however, following decoding the random data is transformed into a known sequence, which can be remodulated or reconstructed into a complex sample-sequence and used as the reference signal $\tilde{s}_i^*(\tau)$ in the delay estimator, as in equation (6).

The CRB depends on the sum of the squared magnitude of the derivative of the reconstructed signal, implying that intervals where the derivative is zero do not contribute to the CRB and hence can be ignored. This suggests that only the intervals around the transitions are relevant. Since the reconstructed signal is identical to the received signal except for a delay, the transition regions can be identified and a window function consistent with the delay uncertainty applied to identify the transition regions in both the received and reconstructed signals, in order to reduce the noise before the correlation operation of equation (6) is applied. However, since the delay is not known to the required accuracy in advance, the width of the window must be adjusted to be consistent with the uncertainty in the delay estimate.

In order to apply a temporal window much smaller than a symbol-duration, the uncertainty in the true delay must be known to an accuracy smaller than the window to be effective. The window function used in Fig. 8 to improve the performance of BPSK and OQPSK sequences corresponds to 1/50 of a symbol, hence this approach appears to be most suitable for low symbol-rate uplink data. Fig. 8 refers to I-Q modulation for both BPSK and OQPSK signals, instead of phase modulation.

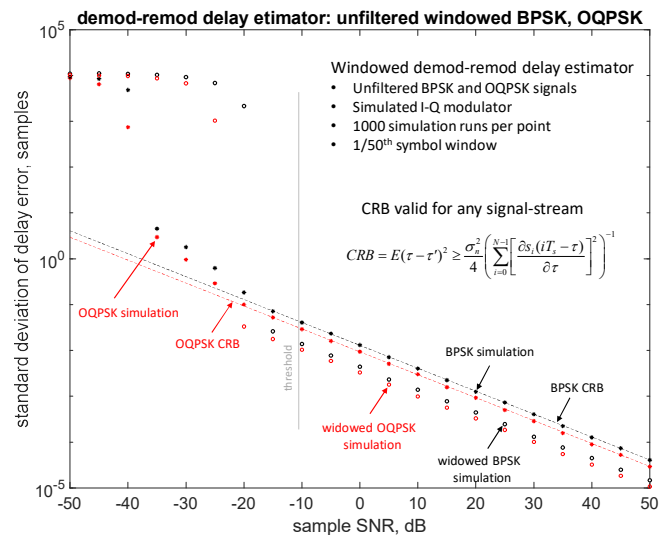


Figure 8. Improved delay estimator performance via windowing: unfiltered BPSK (black) and OQPSK (red); IQ modulation.

9. END-TO-END RANGING ACCURACY

In this example, an initial assessment of the performance of the Telecommand/Telemetry Ranging (TC/TM Ranging) system operating under realistic conditions will be investigated. This assessment is limited to analysis of the tracking loop performance based on signal to noise ratios, and does not include other practical losses such as calibration errors.

The ranging information contained in the command sequence is condensed into a single delay measurement at the spacecraft, and transmitted to the ground as part of the information in a data codeword. Hence all of the power available for communication can be allocated to the data channel when suppressed carrier modulation is used, or it can be balanced between the residual carrier and the data modulation on the downlink.

The critical functions required to implement the TCBR concept consist of measuring the code-delay of the uplink command sequence, incorporating the measured command delay into a downlink codeword, then recovering the command delay on the ground together with a simultaneous measurement of the codeword delay at the ground receiver. The receiver on the ground acquires and tracks the received carrier, followed by codeword demodulation, detection and decoding. Since the received codewords contain random binary symbols, hence do not have the near-periodic structure of the compound PN code observed at the spacecraft, a digital data-transition tracking loop (DTTL) or equivalent must be used to establish symbol synchronization at the ground receiver. For ranging applications, an estimate of the arrival-time of the codeword symbols is required to complete the two-way delay calculation, hence errors in the DTTL symbol synchronization loop contribute directly to the total delay error on the ground.

The theoretical performance of the end-to-end TCBR system is determined by evaluating the Cramer-Rao bound on symbol synchronization, assuming that losses due to carrier phase fluctuations can be ignored, both at the spacecraft and on the ground, since under nominal operating conditions there is sufficient SNR to enable accurate carrier tracking. A model for the average effective power of the signal in both the command delay estimator on the spacecraft and the symbol tracking loop on the ground is developed, and applied to the CRB for command and symbol synchronization to obtain the average CRB characterizing the cascade in both the spacecraft and ground receivers. Since the errors in the spacecraft and on the ground are independent, the variance of the total two-way delay error can be calculated by adding the variance of the delay errors on the spacecraft and at the ground receiver. In this development, we can equivalently add the average CRB of the ground and spacecraft receivers, because the averaged CRBs are lower bounds on the delay error variance and hence add for independent processes.

The DTTL multiplies a noisy transition estimate with a noisy

error estimate, resulting in a squaring loss S_L as described in [2]. Windowing in the DTTL improves noise performance, effectively reducing the noise power by a factor of W . As shown in [2], the squaring loss for the DTTL is given by the following expression:

$$S_L = \frac{2 \left[\operatorname{erf}(\sqrt{R_s}) - \frac{W}{2} \sqrt{\frac{R_s}{\pi}} \exp(-R_s) \right]^2}{W \left\{ 1 + \frac{WR_s}{2} - \frac{W}{2} \left[\frac{1}{\sqrt{\pi}} \exp(-R_s) + \sqrt{R_s} \operatorname{erf}(\sqrt{R_s}) \right]^2 \right\}} \quad (12)$$

where $R_s = PT_c / N_0$, and T_c is the symbol duration in seconds. Taking both windowing and squaring loss into account, the CRB can be expressed in terms of samples as

$$\sigma_d^2 \equiv \operatorname{var}(\tau - \hat{\tau}) = \frac{WB_L}{2S_L P / N_0} \quad (13)$$

where S_L is defined in equation (12), and B_L is the closed-loop bandwidth of the DTTL. In the high-SNR limit the transition estimates are essentially noise-free hence there is no squaring-loss, $S_L \rightarrow 1$, and the CRB for the DTTL can be expressed as

$$\sigma_d^2 \cong \frac{WB_L}{2P / N_0} \quad (14)$$

In the low-SNR limit $R_s \rightarrow 0$, $S_L \rightarrow 2R_s / W$, and the low-SNR CRB can be approximated as

$$\sigma_d^2 \cong \frac{W^2 B_L}{2R_s (P / N_0)} \quad (15)$$

The CRB derived in equation (11) is a lower bound on the variance of the delay estimate on the uplink channel, re-defined here as

$$\sigma_u^2 \geq \frac{\sigma_n^2}{4} \left(\sum_{i=0}^{N-1} \left| \frac{\partial \tilde{s}_i(\tau)}{\partial \tau} \right|^2 \right)^{-1} \quad (16)$$

Since the delay measurements in the uplink and downlink parts of the link are independent, the variance of the two-way range error, σ_{ud}^2 , can be expressed as the sum of the uplink and downlink range error variances: $\sigma_{ud}^2 = \sigma_u^2 + \sigma_d^2$. Fig. 8 is a plot of the end-to-end delay error variance σ_{ud}^2 , showing the delay error variance in the three regions defined in Section IV.

The simulation points for the end-to-end channel (shown by the red asterisks in Fig. 9) have been obtained by adding the simulation points for the uplink channel described in Section VII, to the asymptotic bounds on downlink error performance, equations (14) and (15), expressed in symbol-SNR as customary in synchronization systems. Note that the low-SNR performance of the end-to-end system is degraded by the squaring loss inherent in the DTTL implementation, in addition to the effects described in Section VII.

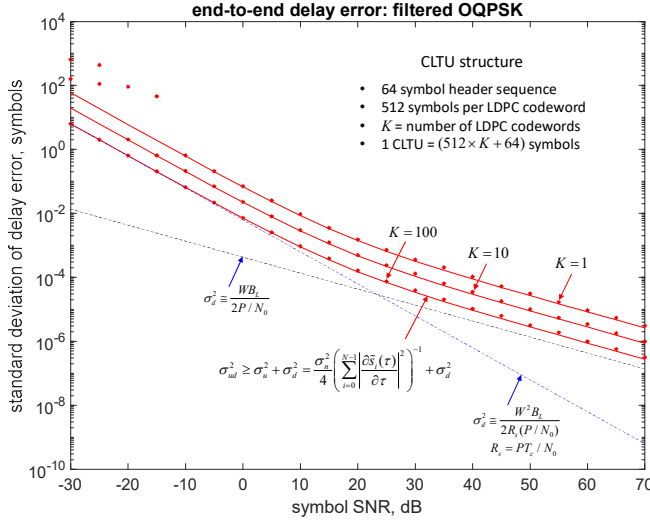


Figure 9. End-to-end rms delay error with filtered OQPSK signals in symbols, as a function of symbol-SNR, for K = 1, 10 and 100 LDPC codewords per CLTU: downlink DTTL high-SNR bound (dashed green); downlink DTTL low-SNR squaring loss bound (dashed blue); uplink CRB (dashed black); end-to-end bound (solid red); simulation (red asterisks).

Synchronization systems are often characterized in terms of symbol-SNR instead of sample-SNR, which is a simple conversion in dB: symbol-SNR is sample_SNR times the number of samples per symbol. For example, with 100 samples/symbol, the symbol-SNR becomes sample-SNR in dB + 20 dB: therefore 0 dB sample-SNR in Fig. 8 corresponds to 20 dB symbol-SNR.

Range R in meters (m) and delay τ in seconds (s) are related as $R = c\tau$, where c is the speed of light in m/s. In the context of symbol synchronization, delay is often specified in fractional symbols, which makes it easy to convert from delay to range using the known symbol-rate (symbols/second) for a given link. For example, at a sampling rate of 1 MSPS, the rms delay error of the end-to-end system at 20 dB symbol-SNR (or equivalently 0 dB sample-SNR) is approximately 0.1 samples rms, when a CLTU consisting of 1000 symbols is employed. This, in turn, corresponds to an rms range error of $\Delta R = c\Delta\tau = (3 \times 10^8)(10^{-7}) = 30$ meters, which is too large for deep-space ranging applications, where sub-meter ranging accuracies are required.

More realistic examples can be constructed using the structure of the CLTU described in Section II, based on the CCSDS requirements in [7]. Assuming long LDPC codewords with 512 symbols each, and a header sequence of 64 symbols, a CLTU consists of $512 \times K + 64$ symbols without a tail-sequence (optional for LDPC codes). Assuming identical uplink and downlink data-rates, the rms range error is shown in Fig. 8 as a function of symbol-SNR for $K = 1, 10$ and 100 LDPC codewords per CLTU.

It can be seen in Fig. 8 that with $K = 100$ LDPC codewords per CLTU, processing over a single CLTU yields an rms error of 9×10^{-4} symbols at a symbol-SNR of 10 dB. The range

equation can be formulated in terms of fractional symbol error by writing the delay in symbols divided by a scaling factor with dimensions of symbols/second: $\Delta R = c\Delta\tau_s s_\tau^{-1}$, where τ_s is delay in symbols, and s_τ is the scaling factor in units of symbols/second. For example, at a symbol rate of 1 MSPS, the scaling factor is $s_\tau = 10^6$ symbols/seconds, which yields an rms range error of $\Delta R = c\Delta\tau_s s_\tau^{-1} = (3 \times 10^8)(9 \times 10^{-4}) \times 10^{-6} = 27 \times 10^{-2}$ m, or 0.27 meters. This is sufficient to meet DSN ranging requirements, implying that uplink data or commands of 1 MSPS or higher symbol-rates are sufficient to meet DSN ranging requirements with symbol-SNR of 10 dB.

At much lower symbol-rates, as would be the case at extreme interplanetary distances or emergency commands, the symbol-SNR would decrease resulting in a corresponding increase in ranging accuracy. This effect can be mitigated via windowing that yields an improvement of approximately 10 dB when the window is 1/50 of a symbol is applied, as shown in Fig. 7, assuming that the range uncertainty is suitably small. For example, at a symbol-rate of 10 kSPS (1/100th of the 1 MSPS example described above), the scaling factor is $s_\tau = 10^4$ symbols/second. At a symbol-SNR of 15 dB, slightly higher than for the high symbol-rate example, the rms range error from Fig. 9 becomes $\Delta R = c\Delta\tau_s s_\tau^{-1} = (3 \times 10^8)(3.5 \times 10^{-4}) \times 10^{-4} = 10.5$ meters, which is too large for DSN applications. However, using windowing as described in Section VIII, the rms delay error can be reduced by approximately 10 dB to an acceptable level of roughly 1 meter rms, meeting DSN requirements.

10. SUMMARY AND CONCLUSIONS

The end-to-end delay and range estimation performance of telemetry based two-way deep-space communications links was investigated in this paper, relying on the demod-remod capabilities of future deep-space transponders, as outlined in CCSDS documents [7]. The demod-remod feature in advanced spacecraft transponders decodes and reconstructs the received random data, transmitted in a CCSDS specified CLTU, effectively transforming the random data components of the CLTU into known waveforms. The maximum likelihood algorithm for delay estimation with arbitrary but known waveforms was derived along with the Cramer-Rao bound on delay estimation error, and MATLAB simulations performed using BPSK and OQPSK data to validate the analysis results. A pre-correlation windowing approach was developed, indicating that up to 10 dB improvement in delay estimation error may be obtained, if the delay uncertainty can be reduced to a small fraction of a symbol, thus benefiting delay estimator performance at low data-rates. It was shown that ranging errors of less than a meter can be achieved with symbol-SNRs of 10 dB or more, when 100 or more LDPC codewords of length 512 symbols are contained in each CLTU, or when several consecutive smaller CLTUs totaling the same number of symbols are used to make a delay

estimate, meeting NASA requirements for deep-space ranging accuracy.

ACKNOWLEDGEMENTS

The authors thank Gunther Sessler for suggesting that the telemetry ranging concept may be extended to TC/TM ranging by replacing the uplink PN transmission with a telecommand signal.

This research was carried out at the Jet Propulsion Laboratory, California Institute of Technology, under a contract with the National Aeronautics and Space Administration.

Copyright 2018 California Institute of Technology. U.S. Government sponsorship acknowledged.

REFERENCES

- [1] Hamkins, J., P. Kinman, H. Xie, V. Vilnrotter, and S. Dolinar, "Telemetry Ranging: Concepts," IPN PR 42-203, pp. 1-20, November 15, 2015.
- [2] Hamkins, J., P. Kinman, H. Xie, V. Vilnrotter, and S. Dolinar, "Telemetry Ranging: Signal Processing," IPN PR 42-204, pp. 1-56, February 15, 2016.
- [3] Hamkins, J., P. Kinman, H. Xie, V. Vilnrotter, S. Dolinar, N. Adams, E. Sanchez, and W. Millard, "Telemetry Ranging: Laboratory Validation Tests and End-to-End Performance," IPN PR 42-206, pp. 1-35, August 15, 2016.
- [4] "Sequential Ranging," DSN Telecommunications Link Design Handbook, Document 810-005, Module 203, Rec. C, 2009.

BIOGRAPHY



Victor Vilnrotter (M'79, SM'02) received his Ph.D. in electrical engineering and communications theory from the University of Southern California in 1978. He joined the Jet Propulsion Laboratory, Pasadena, Calif., in 1979, where he is a Principal Engineer in the Communications Architectures and Research section. His research interests include electronic compensation of large antennas with focal-plane arrays, adaptive combining algorithms for antenna arrays, optical communications through atmospheric turbulence, the application of quantum communications to deep-space optical links, and the development of uplink array calibration and tracking technologies. He has published extensively in conferences and refereed journals, and has received numerous NASA awards for technical innovations.